STATE OF THE CLIMATE IN 2011

Special Supplement to the
Bulletin of the American Meteorological Society
Vol. 93, No. 7, July 2012

STATE OF THE CLIMATE IN 2011

Editors

Jessica Blunden

Derek S. Arndt

Associate Editors

Howard J. Diamond

A. Johannes Dolman

Ryan L. Fogt

Margarita C. Gregg

Bradley D. Hall

Martin O. Jeffries

Michele L. Newlin

James A. Renwick

Jacqueline A. Richter-Menge

Ahira Sánchez-Lugo

Ted A. Scambos

Wassila M. Thiaw

Peter W. Thorne

Scott J. Weaver

Kate M. Willett

AMERICAN METEOROLOGICAL SOCIETY

6. ANTARCTICA—R. L. Fogt and T. A. Scambos, Eds.

a. Overview—R. L. Fogt and T. A. Scambos

Antarctica's climate in 2011 appears to have been marked by a quiet start and a relatively intense ending. Annual mean surface pressure anomalies and 2 m temperature anomalies based on ERA-Interim are displayed in Figs. 6.1a and b, respectively, with the shading denoting how many standard deviations these anomalies were from the 1981–2010 mean. ERA-Interim was employed since it is a newer higher resolution (both horizontally and vertically) reanalysis that uses a four-dimensional variational assimilation scheme; further, ERA-Interim has proven to perform better than other reanalyses across Antarctica (Bromwich et al. 2011). Despite Fig. 6.1 indicating above-average surface pressures and temperatures (with the exception of the Weddell Sea) throughout the year over Antarctica, monthly circulation patterns were generally unremarkable until December (actually beginning in the last weeks of November) when more intense low pressures, and in particular a strong low in the Amundsen Sea, led to widespread cooler conditions and resulted in the highest southern annular mode (SAM) index on record for December [+3.53 based on the Marshall (2003) SAM index and +2.573 based on the NOAA CPC SAM index]. The late period was also marked by a strong zonal wavenumber-3 (ZW3) component to the circulation. These patterns occurred during the height of the 2011/12 field season and caused several disruptions and inconveniences, particularly in West Antarctica.

Notable Antarctic climate events during 2011 include:

- Winter and spring temperature anomalies exceeding +3°C over much of the Antarctic continent, more than 2 standard deviations above the long-term mean;
- Below-normal winter temperatures in the northern Antarctic Peninsula, which continued the downward trend there during the last 15 years, effectively stabilizing the temperature trend during the last 30 years;
- A sea ice extent anomaly which increased steadily through much of the year, from a brief record-setting low in April, to well above average in December, the latter trend reflecting the dispersive effects of low pressure systems on sea ice, and generally cool conditions around the Antarctic perimeter;
- Surface melt that was still moderately below normal, but greater than the past two summer seasons (for melt, the 2010/11 austral summer, not the most recent summer, is reviewed since the year's analysis begins at the calendar year end);
- Greater-than-average precipitation along the Dronning Maud Land coast, but generally lower than average along the Bellingshausen Sea coast;
- An extensive, deep, and persistent ozone hole in September, indicating that, while not worsening currently, the recovery to pre-1980 conditions is proceeding very slowly; and
- An all-time record high temperature of -12.3°C observed for South Pole station (on 25 December), exceeding the previous record by more than a full degree.

In October, NASA scientists also noticed that a major fracture, or rift, appeared in the large Pine Island Glacier Ice Shelf, several kilometers further upstream than previous rifts (as monitored over the past 30 years). The new rifting is likely a result of changing stress conditions due to basal melt of the ice and thinning, and the recent retreat of the grounding line. The glacier, already significantly out of balance (more outflow than incoming snowfall) and accelerating, will probably see a further increase in flow speed as a result.

The climatological averages referenced in this chapter refer to the mean conditions during 1981–2010 period, unless otherwise specified.

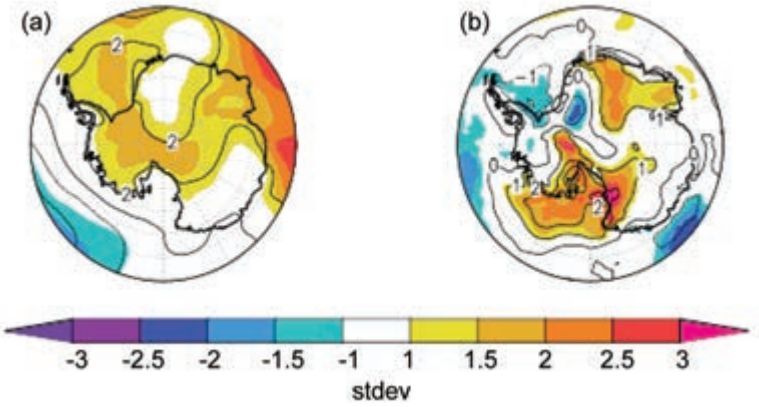

Fig. 6.1. 2011 Annual mean (a) surface pressure (hPa) and (b) surface temperature (°C) anomalies based on the ERA-Interim reanalysis. The shading represents how many standard deviations the anomalies are from the 1981–2010 mean (color bar at bottom for scale). Contour interval is 2 hPa for (a) and 1°C for (b).

b. Circulation—A. J. Wovrosh, S. Barreira, R. L. Fogt, and T. A. Scambos

Antarctic and southern high-latitude circulation features during 2011 were characterized by mild to moderate patterns until late in the year, when an intense Amundsen Sea Low (ASL) and strong zonal wavenumber-3 (ZW3) pattern emerged, although with the ridge and trough locations westward displaced compared to Raphael (2004). Figure 6.2 presents a vertical cross section extending from the troposphere to the stratosphere of geopotential height and temperature anomalies averaged over the polar cap (60°S–90°S), as well as circumpolar (50°S–70°S) averaged zonal wind anomalies. The year was then divided into parts for which consistent circulation anomalies were observed, namely January–April, May–June, July–November, and December. For each of these periods, mean surface pressure and surface temperature anomalies are plotted in Fig. 6.3 to highlight the spatial circulation patterns. In all cases, the period 1981–2010 was used to calculate the climatological mean and standard deviation. Similar results are obtained with the NCEP-NCAR reanalysis, although the higher spatial resolution (both horizontal and vertical) of ERA-Interim allows for more features to be distinguished, particularly in the temperature field and throughout the stratosphere. The use of reanalyses or other gridded products is necessary to fill in the gaps between the sparse observational network; 2011 Antarctic climate anomalies from direct observations are discussed in section 6c.

The year began with comparatively weak geopotential height anomalies throughout the troposphere and stratosphere during January–April (Fig. 6.2). February stands out with stronger-than-average circumpolar zonal winds in the upper troposphere (~50 hPa – 200 hPa), primarily driven by a strong high pressure in the Indian Ocean sector (apparent in the January–April mean in Fig. 6.3a). In the Antarctic interior, surface pressure anomalies were near normal in May–June (Fig. 6.3c), with a few colder-than-average regions in East Antarctica, and warmer-than-average temperatures in the South

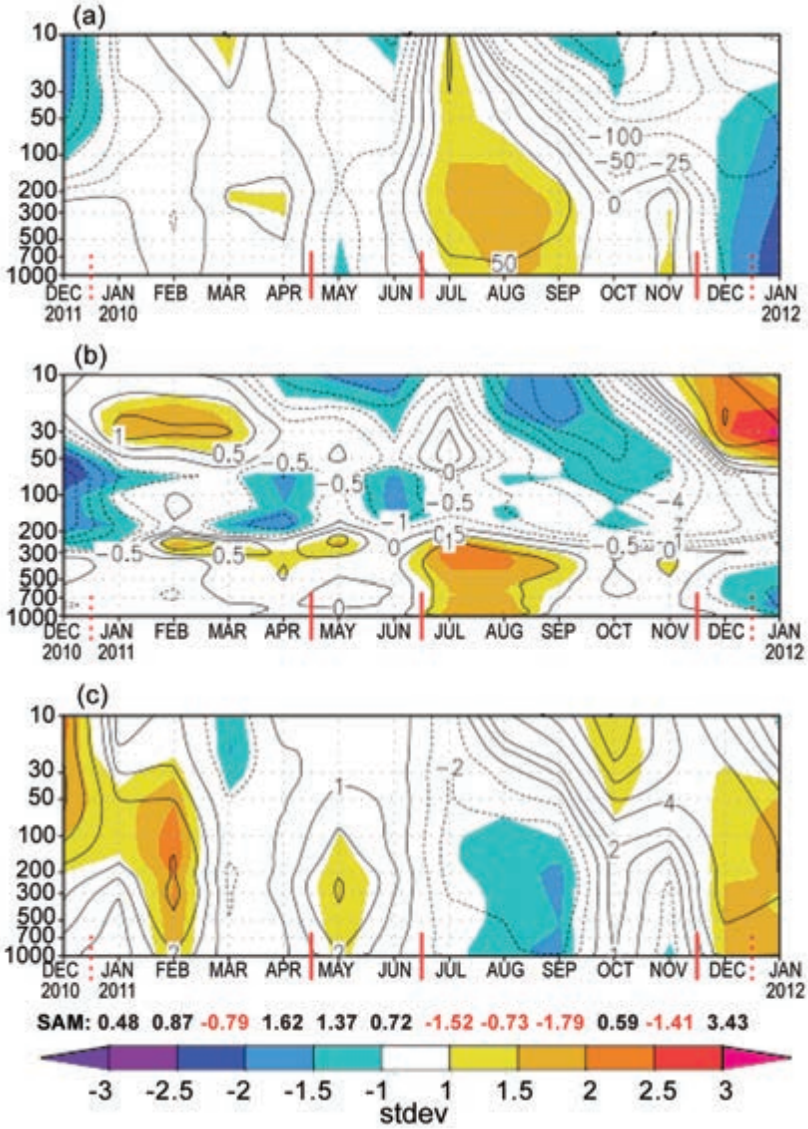

Fig. 6.2. Zonally averaged climate parameter anomalies for the southern polar region in 2011 relative to the 1981–2010 period: (a) polar cap (60°S–90°S) averaged geopotential height anomalies (m); (b) polar cap averaged temperature anomalies (°C); (c) circumpolar (50°S–70°S) averaged zonal wind anomalies (m s^{-1}). The shading represents how many standard deviations the anomalies are from the 1981–2010 mean, as in Fig. 6.1. Red vertical bars indicate the four separate climate periods shown as spatial climate anomalies in Fig. 6.3; the dashed lines near December 2010 and December 2011 indicate circulation patterns wrapping around the calendar year. Primary contour interval is 50 m in (a), 1°C in (b), and 2 m s^{-1} in (c), with additional contours at ±25 m, ±0.5°C, and ±1 m s^{-1} in (a), (b), and (c), respectively. Values for the SAM index are shown along the bottom in black and red. (Source: ERA-Interim reanalysis.)

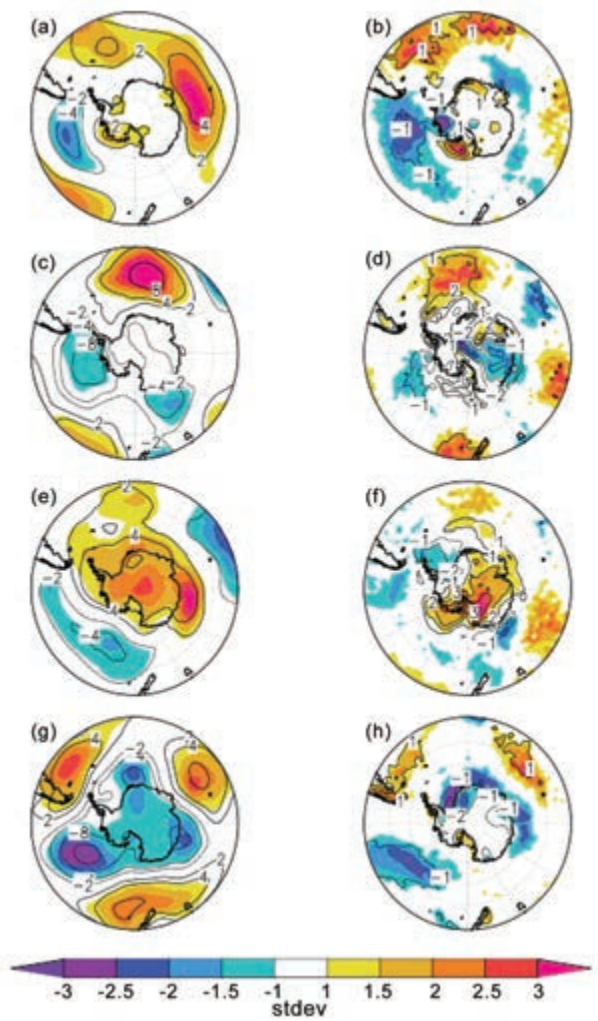

Fig. 6.3 (left) Surface pressure anomaly and (right) 2 m temperature anomaly contours (every 4 hPa with an additional contour at ±2 hPa and every 1°C, respectively, zero contours emitted) relative to 1981–2010 climatology for (a) and (b) January–April 2011; (c) and (d) May–June 2011; (e) and (f) July–November 2011; (g) and (h) December 2011. The shaded regions correspond to the number of standard deviations the anomalies are from the 1981–2010 mean, as in Fig. 6.1. (Source: ERA-Interim reanalysis.)

Atlantic (Fig. 6.3d). More distinguishable during this period were the below-average temperatures in the polar stratosphere (Fig. 6.2b), which generally persisted until December.

The austral winter and spring seasons (July–November) were marked by high surface pressure (Fig. 6.3e) and associated above-average geopotential heights throughout the troposphere (Fig. 6.2a). Surface temperatures were also well above normal for all but the Antarctic Peninsula (Fig. 6.3f). These temperature anomalies exceeded 3°C for much of the Antarctic continent, and were more than two standard deviations above the 1981–2010 mean. The circumpolar zonal winds were weaker than average during much of this time, although the SAM index was never strongly negative (never < -2). Examining the monthly circulation anomalies, the pattern was similar to ZW3 throughout much of the winter, especially in August (not shown separately). During this month, strong ridges were observed at 45°E, 150°E, and 60°W, and the meridional flow associated with this led to the intrusion of many warm air masses in that month, significantly warming the continental areas to the west of these longitudes.

In December, the circulation pattern switched dramatically. As heights fell over Antarctica (Fig. 6.2a), surface pressures dropped (Fig. 6.3g), and the above-average temperatures diminished to near normal or below average over the continent (Fig. 6.3h). Overall, the circulation pattern was again dominated by ZW3 (Raphael 2004), but the location of the alternating trough and ridge waves were rotated westward. The Amundsen Sea Low (ASL) was very deep and extensive, with central pressures as much as 12 hPa (or > 2.5 standard deviations) below the mean. The ASL center was also shifted significantly northwestward (to ~150°W, see Fig. 6.3g), leading to a shift in the location of the air temperature anomalies associated with a strong ASL. The intense and shifted pattern of pressure in December (actually beginning in the second half of November) led to severe logistical problems with several major US field research campaigns. At the WAIS Divide camp (79.5°S, 112.1°W), nine intense storms were recorded between early December and mid-January 2012; at Pine Island camp (75.8°S, 100.3°W), persistent poor weather resulted in a five-week delay in science activity, and the season had to be abbreviated when weather did not improve in January. Although the SAM index reached a new high record in December, the deep ASL and the alternating wave-train of pressures extending from New Zealand towards southern South America are more reminiscent of the Pacific South American pattern and the resurgence of La Niña in the autumn of 2011.

c. *Surface manned and automatic weather station observations*—S. Colwell, L. M. Keller, and M. A. Lazzara

The Antarctic climate extremes over 2011 are reflected in observations at staffed and automatic weather stations (AWS). A map of key locations described in this section and throughout the chapter is displayed in Fig. 6.4. Climate data from two representative staffed stations (Rothera and Vostok) and

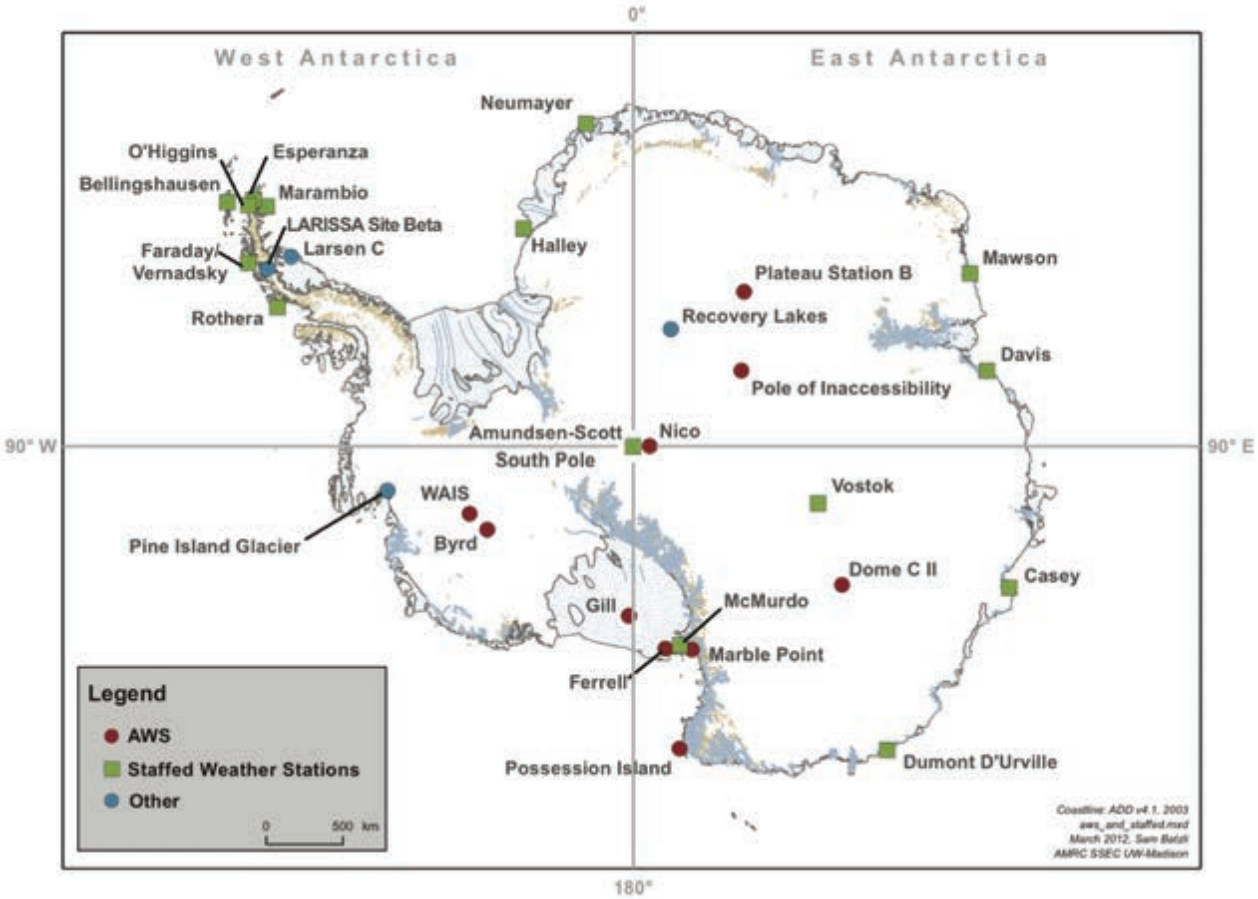

Fig. 6.4. Map identifying locations of automatic and staffed Antarctic weather stations described in chapter 6.

two automatic stations (Byrd and Gill) are displayed in Figs. 6.5a–d. At the staffed stations, wind speeds were near normal throughout the year, reflected in Figs. 6.5a–b.

Monthly mean temperatures on the western side of the Antarctic Peninsula were near average for most of the year. However, temperatures at Marambio station on the eastern side were below average for most months, and many stations on the northern Antarctic Peninsula experienced a cool winter, with temperatures around 4°C – 5°C below the 1981–2010 climatology in much of July–September, reflected in Figs. 6.1a and 6.3f. The Antarctic Peninsula region as a whole experienced significantly high pressures during July and August (reflected in Fig. 6.3e), with Rothera station recording a record mean August pressure of 1001.7 hPa, 14.8 hPa above the long-term mean (Fig. 6.5a).

In the Weddell Sea and Dronning Maud Land region, monthly mean temperatures at Halley and Neumayer stations fluctuated around the long-term mean for most of the year, consistent with the weak annual mean temperature anomalies there (Fig. 6.1b). High monthly mean pressures were recorded at both stations from July to September, with very low pressures (> 8 hPa below average) in December. Around the Indian Ocean coast of East Antarctica, the monthly mean temperatures at Mawson, Davis, and Casey similarly tended to oscillate around the mean, with temperatures more than 4°C above the long-term mean recorded at Davis and Mawson in July, consistent with the warm air advection of the ZW3 influence described in the previous section. In December, all three stations recorded pressures more than 5.5 hPa below the long-term mean, reflecting the dramatic change in circulation at this time.

Reviewing the East Antarctic interior, monthly mean temperatures at Vostok station (Fig. 6.5b) were generally above average, with a new record monthly mean of -60.6°C being set in August, 7.5°C above the long-term mean. Overall, 2011 was the second warmest year on record at Vostok with an annual mean temperature of -53.5°C. Interestingly, the Dome C II station had a record low monthly mean temperature (-7.6°C below normal) for June, but more normal conditions for July and August. At Amundsen-Scott South Pole station, the temperatures varied over the year, sometimes significantly above average and

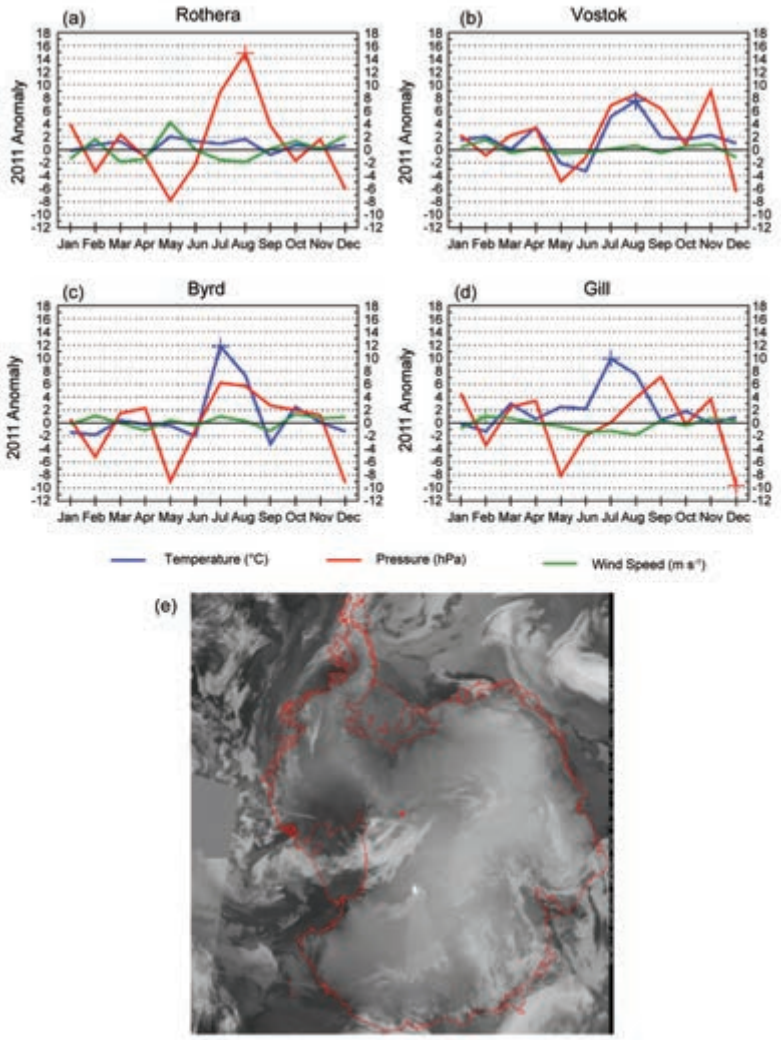

Fig. 6.5. (a)–(d) 2011 Antarctic climate anomalies at four representative stations (two staffed, two automatic). Monthly mean anomalies for temperature (°C), MSLP (hPa), and wind speed (m s^{-1}) are shown, with plus signs (+) denoting record anomalies for a given month at each station in 2011. Climatological data start in 1976 for Rothera, 1958 for Vostok (with some gaps), 1980 for Byrd, and 1985 for Gill. The base period for calculating anomalies was 1981–2010 for the staffed stations, and the full period of observation for the automatic stations. (e) Satellite mosaic of thermal-band emission on 25 December 2011, date of an all-time record high temperature at South Pole (-12.3°C). The red dot shows the location of Amundsen-Scott South Pole station.

sometimes below. In May, the mean temperature was 4.8°C below average, at -62.6°C, the coldest May average ever recorded. In December, the monthly mean temperature was about average but a new record maximum temperature (for any month) of -12.3°C was recorded on 25 December. Multiple AWS records near the South Pole confirmed the record warmth, for example, Nico AWS (100 km grid east of the pole) set a record of -8.2°C for the same day. A satellite thermal infrared image from that day (Fig. 6.5e) shows warm conditions in both the Ross Embayment and the southernmost Ronne Ice Shelf areas, and a series of lows moving inland and southwards across the Ross Ice Shelf.

West Antarctica and the Ross Sea embayment also saw record warmth in July with AWS units Ferrell, Byrd (Fig. 6.5c), Marble Point, Possession Island, and Gill (Fig. 6.5d) all reporting record high monthly temperatures (approximately -6°C along the Ross Sea coast; -11.8°C at Byrd). Possession Island also reported record high monthly mean temperatures for February, June, and August.

The AWS units on the Ross Sea and Ross Ice Shelf had above-normal monthly mean temperatures for most of 2011, reflected in the local maximum temperature anomaly there in Fig. 6.1b. As a result, Ferrell, Gill, Marble Point, and Possession Island all observed their warmest annual mean in 2011. Dome C II also had above-normal temperatures for most of the year, while Byrd was slightly below normal for most of the year. Even though temperatures were quite warm, the wind speeds were close to normal for the year for most of the AWS units. The exceptions occurred in February where Gill tied the record maximum wind speed (Fig. 6.5d) and Dome C II was 0.2 m s^{-1} below the record maximum wind speed. All the stations from Byrd across the Ross Ice Shelf to Dome C II had unusually low mean pressure (around 6 hPa – 7 hPa below normal) for May (Fig. 6.5c). Near-record or record low pressure occurred in December at all of the AWS units discussed here, with pressures around 8 hPa – 9 hPa below normal. Gill reported a record low December mean pressure of 973.1 hPa, 9.6 hPa below normal (Fig. 6.5d). As noted above, coastal stations in East Antarctica also had very low pressures in December, reflecting the regional circulation anomalies that are part of the deep ASL, record positive SAM, and strong ZW3 pattern at this time (Fig. 6.2g).

d. Net precipitation (P–E)—D. H. Bromwich and S.-H. Wang

Precipitation minus evaporation (P–E) closely approximates the surface mass balance over Antarctica, except for the steep coastal slopes (e.g., Bromwich et al. 2000; van den Broeke et al. 2006). Precipitation variability dominates P–E changes over the Antarctic continent. Precipitation and evaporation/sublimation fields from the Japanese reanalysis (JRA; Onogi et al. 2007) were examined to assess Antarctic net precipitation (P–E) behavior for 2011. The evaporation in JRA was calculated from the surface latent heat flux variable. In comparisons to other long-term global reanalyses (e.g., NCEP1 and NCEP2), JRA has higher model resolution, both horizontally and vertically, greater observational usage, and a more advanced model configuration (Onogi et al. 2007; Bromwich et al. 2007). Nicolas and Bromwich (2011) show that the reliability of JRA P–E is highly ranked in relation to other global reanalyses.

Figures 6.6a–d show the 2011 JRA annual and austral fall (MAM) anomalies of P–E and mean sea level pressure (MSLP). In general, the annual anomalies over the high interior of the continent were small (within ±50 mm yr^{-1}), consistent with the low values of snow accumulation in this region. Most coastal regions in 2011 displayed opposite P–E anomalies to

SIDEBAR 6.1: RECENT COOLER CONDITIONS ON THE NORTHERN ANTARCTIC PENINSULA—D. MCGRATH AND K. STEFFEN

Atmospheric warming over the Antarctic Peninsula (AP) during the second half of the 20th century was remarkable, with local trends exceeding 0.5°C $decade^{-1}$ (Vaughan et al. 2003; Turner et al. 2005). The complexity of the atmospheric and oceanic circulation around the AP precludes clear attribution of this warming, although modified circulation patterns, largely driven by changes in latitudinal pressure gradients measured by the southern annular mode (SAM) index (Vaughan et al. 2001; Marshall 2003), likely played an important role (Thompson and Solomon 2002; van den Broeke and van Lipzig 2004). There has been increased advection of warm, maritime air towards the AP, and subsequently, an increased upwelling of Circumpolar Deep Water (CDW) onto the continental shelf of the Amundsen-Bellingshausen Sea (ABS; Orr et al. 2008; Jacobs et al. 2011; Martinson 2011). Dramatic reductions in sea ice extent (-6.6% $decade^{-1}$) in the ABS likely contributed to this warming as well, possibly as a driver and certainly as a positive feedback (Meredith and King 2005; Turner et al. 2009).

This warming has had important glaciological impacts, including widespread glacier front retreat and acceleration along the western margin of the AP and the collapse of the Larsen A and B ice shelves on the eastern edge, the latter being unprecedented during the Holocene (Pritchard and Vaughan 2007; Scambos et al. 2003; Cook and Vaughan 2010; Domack et al. 2005). A key mechanism in the final collapse of these ice shelves has been the propagation of surface meltwater-filled crevasses through the ice shelf, rendering it into a series of narrow, elongated icebergs (Scambos et al. 2003). This process is dependent on having sufficient surface meltwater, and thus is directly tied to the intensity and duration of surface melting on the ice shelf.

Increased surface melting on the Larsen B Ice Shelf, just prior to its collapse, resulted from strong northeasterly and westerly winds, the latter associated with strong föhn flow over the Peninsula, bringing dry, adiabatically warmed air over the ice shelf (van den Broeke 2005). An increase in this phenomenon is attributed to the increased speed of the circumpolar westerlies, associated with the positive polarity of the SAM index. This atmospheric pattern is characterized by more air passing over, rather than being blocked by, the orography of the Peninsula (Orr et al. 2004, 2008; Marshall 2003).

In contrast to the strong warming trends observed during the previous half-century, between 2000 and 2011, AP stations have shown much greater variability, with many stations showing a slight cooling trend (Fig. SB6.1a; Table SB6.1). The mean annual temperature trend at Marambio station switched from a warming of +0.65 ± 0.47°C $decade^{-1}$ between 1971 and 2000 to a cooling of -1.57 ± 2.4° C $decade^{-1}$ between 2000 and 2011. The cooling has been strongest at other northern AP stations (Bellingshausen, O'Higgins, Esperanza), with a cooling trend of about -0.7°C $decade^{-1}$ over the last 15 years, following a tendency that started with the end of the 1998 El Niño. However, marked cooling is also evident on the Larsen C Ice Shelf, the largest remaining ice shelf on the AP. This site

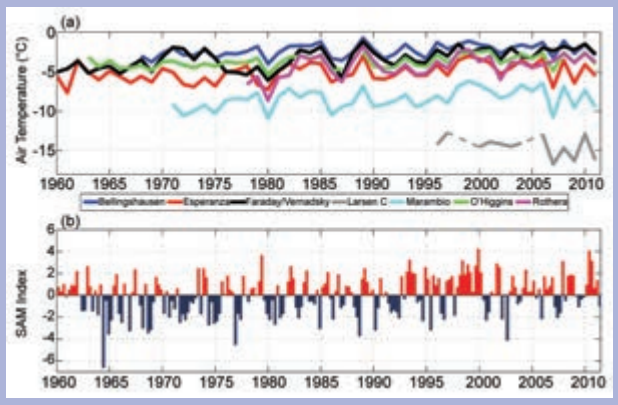

Fig. SB6.1. (a) Mean annual air temperature records (°C) for selected stations on the Antarctic Peninsula. Dashed line for Larsen C indicates incomplete temperature record, precluding calculation of mean annual temperature. (b) Seasonal SAM index calculated from station data (updated from Marshall 2003).

the previous year, especially over the Ross Ice Shelf (between 150°W and 170°E) and Queen Maud Land (between 0° to 50°E). The two strongest negative annual P–E anomalies for 2011 were observed in Wilkes Land (between 90°E and 130°E) and Victoria Land (between 150°E and 170°E), extending the P–E anomaly observed in those regions in 2010 (Bromwich and Wang 2011). The majority of the Ronne Ice Shelf had lower net precipitation in 2011, in contrast to small negative or positive anomalies during 2010.

These annual P–E anomaly features (Fig. 6.6a) were generally consistent with the mean atmospheric circulation implied by the MSLP anomalies (Fig. 6.1a). In 2010 (not shown), negative pressure anomaly centers over the Amundsen-Bellingshausen Sea (~105°W) and the East Antarctic coast (~120°E) produced stronger offshore flow and less precipitation along these regions. During 2011, there was a similar pair of negative pressure anomalies (Fig. 6.1a), but they were weaker and located farther north away from the coast. The positive pressure anomaly over the South Atlantic Ocean during 2010 was extended into the southern Indian Ocean during 2011. The secondary negative anomalies over the Southern Ocean (~45°E) and the Weddell Sea (~30°W) in 2010 were replaced by positive anomalies in 2011. The seasonal P–E

has cooled by -1.11 ± 2.4°C decade^{-1} between 2000 and 2011, although interannual variability is large. It is important to note that none of the reported trends over the past decade are statistically significant, and cooling of a similar magnitude previously occurred over short time periods earlier in the record (Fig. S6.1a). However, with the observed variability over the past decade, there is no longer a statistically significant ($p < 0.05$) warming trend for the northern AP over the last 30 years.

The observed warming from 1950 to 2000, and the more recent temperature variability, cannot be simply and solely attributed to processes associated with the positive trend in the SAM index over this period (Fig. SB6.1b). These processes certainly influence AP climate, and likely contributed to summertime warming of the eastern AP through increased föhn winds on the lee side of the peninsula (Marshall 2007; Orr et al. 2008). However, a significant portion of the regional warming, especially in winter, can be attributed to warming of the central tropical Pacific Ocean and subsequent atmospheric wave trains directed towards West Antarctica (Ding et al. 2011). This likely contributes to increased upwelling of CDW in the Amundsen Sea sector, driving high basal melt rates for glaciers in this region (Steig et al. 2012). The strong negative anomaly in sea ice metrics for the ABS region also has a strong influence on the regional climate (Massom et al. 2008; Stammerjohn et al. 2012), although the exact cause of this negative anomaly is challenging to precisely attribute. The multiple forcing mechanisms therefore both highlight the complexity of the profound changes occurring on the AP and attest to the need for continued research to make accurate predictions for the future.

Table SB6.1. Mean annual air temperature and trends with 95% confidence intervals calculated by standard least-squares linear regression over specified time intervals.

Station Name	Location (°S, °W)	Station Record	Mean Annual Temperature (°C)	Trends to 2000 (°C decade^{-1})	Trends 2000–2011 (°C decade^{-1})
Bellingshausen	-65.4, -64.4	1968–2011	-2.3 ± 0.8	+0.35 ± 0.28	-0.45 ± 1.3
Esperanza	-67.5, -68.1	1945–2011	-5.3 ± 1.3	-0.40 ± 0.19	-1.35 ± 2.2
Faraday/Vernadsky	-62.2, -58.9	1950–2011	-3.7 ± 1.6	+0.59 ± 0.26	+0.37 ± 1.2
Larsen C	-66.9, -60.9	1995–2011	-14.4 ± 1.3	-	-1.11 ± 2.4
Marambio	-63.4, -57.0	1971–2011	-8.5 ± 1.3	+0.65 ± 0.47	-1.57 ± 2.4
O'Higgins	-63.3, -57.9	1963–2011	-3.7 ± 0.8	+0.23 ± 0.21	-0.71 ± 1.5
Rothera	-64.2, -56.7	1978–2011	-4.33 ± 1.4	+1.15 ± 0.94	+0.86 ± 1.6

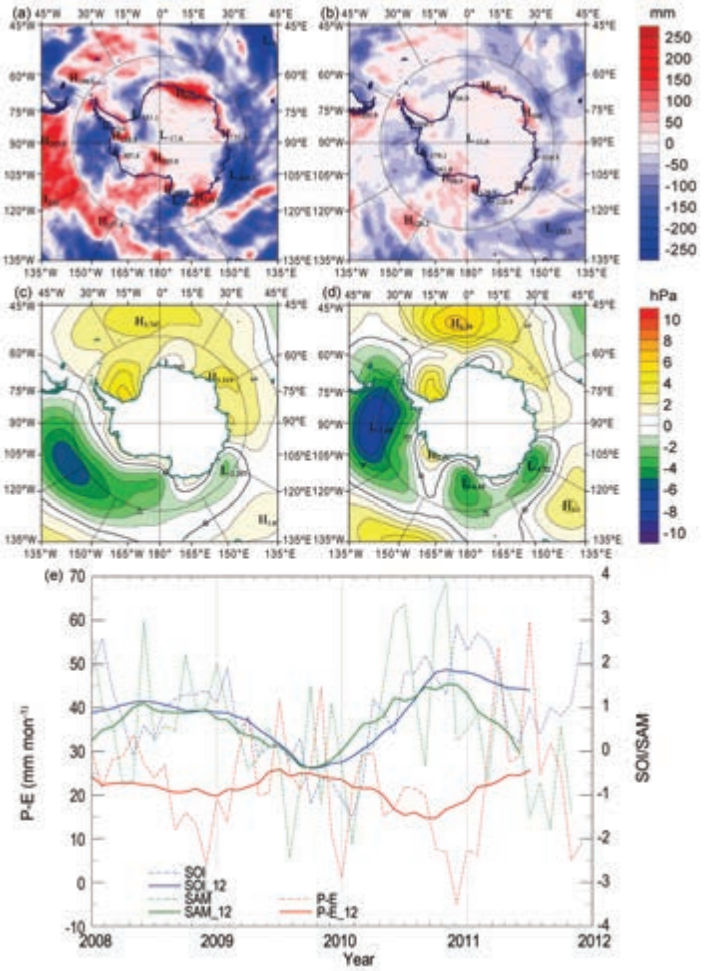

Fig. 6.6. (a)–(d) 2011 annual/seasonal precipitation minus evaporation (P–E; mm) and MSLP (hPa) anomalies departure from the 1981–2010 means: (a) annual P–E anomalies; (b) austral fall (MAM) P–E anomalies; (c) annual MSLP anomalies; and (d) austral fall (MAM) MSLP anomalies. (e) Monthly total P–E (mm; red) for the West Antarctic sector bounded by 75°S–90°S, 120°W–180°, along with the SOI (green, from NOAA's CPC) and SAM (blue, from Marshall 2003) indices since 2008. Centered annual running means are plotted as solid lines.

anomalies can have a large influence on regional annual P–E anomalies. In particular, austral fall values alone contributed more than 50% of the 2011 annual P–E anomalies between the Antarctic Peninsula and the Ross Ice Shelf (60°W to 170°E; Figs. 6.6a–b), and showed good correspondence with austral fall MSLP anomalies (Fig. 6.6d).

The influence of La Niña on P–E also can be observed in Fig. 6.6: from austral fall 2010 to austral winter 2011, negative MSLP anomalies in the Amundsen-Bellingshausen Seas shifted away from the Antarctic coast, ultimately resulting in the large P–E anomaly changes west of the Antarctic Peninsula (from positive to negative) and the Marie Byrd Land-Ross Ice Shelf region (from negative to positive). Earlier studies suggest that those MSLP anomaly features are consistent with simultaneously strong La Niña (Bromwich et al. 2000, 2004) and positive SAM events (Fogt and Bromwich 2006; Fogt et al. 2011). Figure 6.6e shows the time series of average monthly total P–E over the West Antarctica sector (75°S–90°S, 120°W–180°) and monthly SOI and SAM indices (with 12-month running means). It is clear that SOI and SAM are in phase with each other but have opposite behavior to P–E in most months from 2008 onward. The correlation coefficients between monthly P–E and index values are SOI: -0.17 (-0.37 for annual running mean), and SAM: -0.24 (-0.71 for annual running mean). There was also some evidence that the SOI and SAM index are becoming out of phase during later months of 2011.

e. *2010/11 Seasonal melt extent and duration*—L. Wang and H. Liu

Surface snow melt on the Antarctic Ice Sheet during the 2010/11 austral summer was estimated from satellite data using the Special Sensor Microwave/Imager (SSM/I) instrument by applying a wavelet transformation-based edge-detection method (Liu et al. 2005). This tracks melt onset and end dates from the time series of daily brightness temperatures recorded by the horizontally polarized 19 GHz frequency channel. By accumulating the number of days enclosed by melt onset and end pairs during the austral year in the time series, the total number of melt days is calculated for each image pixel. The first and the last melt day in the year were also recorded as the start day of the melt season and the end day of the melt season. Based on these techniques, maps were generated for melt start day (Fig. 6.7a), melt end day (Fig. 6.7b), and annual melt duration (Fig. 6.7c).

As in most years, seasonal melt during 2010/11 was confined almost entirely to the coastal areas. In extremely warm years (such as 2005) some melt signal was observed well inland, e.g., on the Ross Ice Shelf (Liu et al. 2006). However, the 2011 melt season saw almost no melt events in the interior. The total area that experienced surface melt, or melt extent (Torinesi et al. 2003; Liu et al. 2006), was 1 069 375 km^2. This is greater than the previous season (945 000 km^2)

and continues the increasing trend since the 2008/09 season (Wang and Liu 2011). However, the value is still well below the reported average melt extent of the past decades, such as the 26-year (1978–2004) median melt extent (1 277 500 km^2) reported in Liu et al. (2006), and the 20-year mean (1980–99; 1 280 000 km^2) reported in Torinesi et al. (2003). The Melt Index (Zwally and Fiegles 1994; Torinesi et al. 2003; Liu et al. 2006) for austral summer 2010/11, calculated as an annual index by accumulating the number of melting days over a certain area (e.g., the entire Antarctica), was 40 280 625 day·km^2, slightly larger than last year's melt index (39 349 375 day·km^2; Wang and Liu 2011). The melt peak day (Fig. 6.7d) was 29 December 2010, with two smaller peaks in November 2010 and March 2011. The smaller peaks were caused by off-season melt events on the Wilkins Ice Shelf (Figs. 6.7a–b).

Melt area is strongly correlated with latitude; as expected, more melt occurred at lower latitudes than higher ones. Exceptions are the large area of short-period melt on the Ronne-Filchner Ice Shelf, and sporadic melt on Marie Byrd Land (Fig. 6.7c). Extensive melt was seen on the Peninsula, Wilkins, Queen Maud Land, Amery, Shackleton, and Abbot Ice Shelves. Little melt was detected on Ross Ice Shelf, Victoria Land, and Wilkes Land (see Fig. 6.7a for locations). Overall, the melt season of 2010/11 was relatively melt-intensive compared to the past few years in the Antarctic melt record (Tedesco 2009; Tedesco and Monaghan 2009). The magnitude and spatial pattern were similar to those of the previous melt season.

f. Sea ice extent and concentration—R. A. Massom, P. Reid, S. Stammerjohn, S. Barreira, and T. Scambos

During 2011, zonally-averaged Antarctic sea ice extent was characterized by three broad phases that were closely associated with the changes in large-scale patterns of atmospheric circulation described in section 6b.

From near-average levels at the beginning of the year (compared to the 1981–2010 mean), the zonally-averaged sea ice extent tracked at 1–2 standard deviations below the long-term mean from mid-January through mid-May (Fig. 6.8a)—including some brief times when it dipped below the 30-year record. Over this period, negative ice extent anomalies in the (1) eastern Bellingshausen Sea, (2) Weddell Sea (apart from in the southwest), (3) western Amundsen to Ross Seas, and (4) the West Pacific Ocean sector between 75°E and 120°E outweighed strong positive anomalies over much of the eastern Amundsen Sea and the Indian Ocean sector (10°E–70°E; Fig. 6.8b). These positive/negative ice-edge anomalies are likely to be due to a combination of wind-driven ice advection/compaction and in situ thermodynamic growth, the latter associated with the development of cold pools of SST (in the eastern Ross Sea in particular, e.g., in Fig. 6.8d).

The pattern of the 2010/11 season sea ice retreat and advance during the January–May period (not shown) to a large degree reflects the strong positive SAM/La Niña conditions, with generally negative surface pressure anomalies at higher latitudes, particularly in the Amundsen and Bellingshausen Seas, and below-average sea surface temperatures in

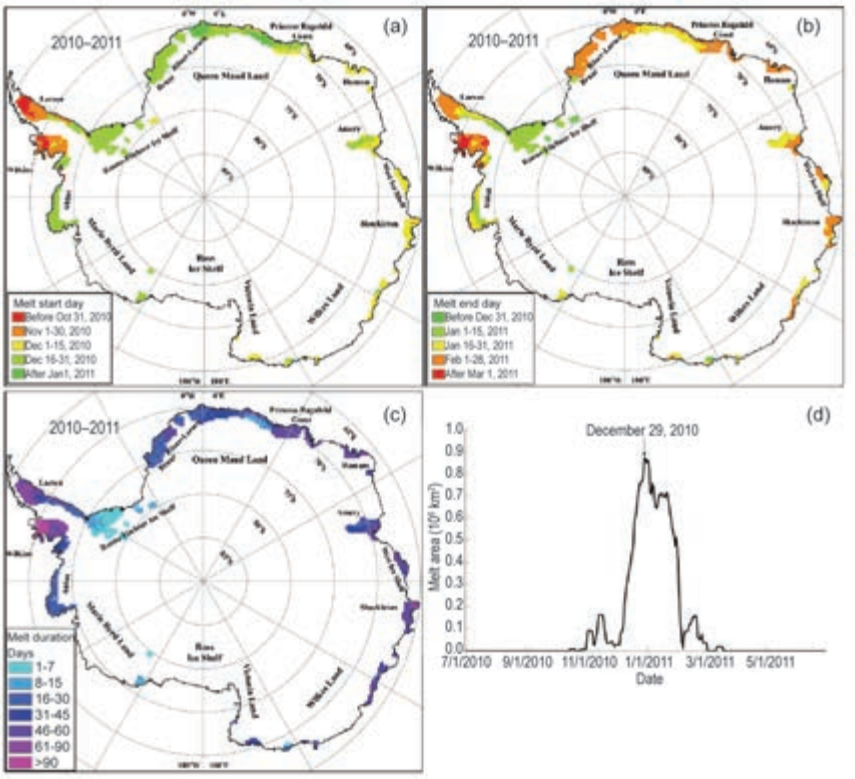

Fig. 6.7. Maps for (a) melt start day, (b) melt end day, and (c) melt duration of Antarctic ice sheet during 2010/11 austral summer. Daily melt extent is shown in (d) with melt peak day indicated.

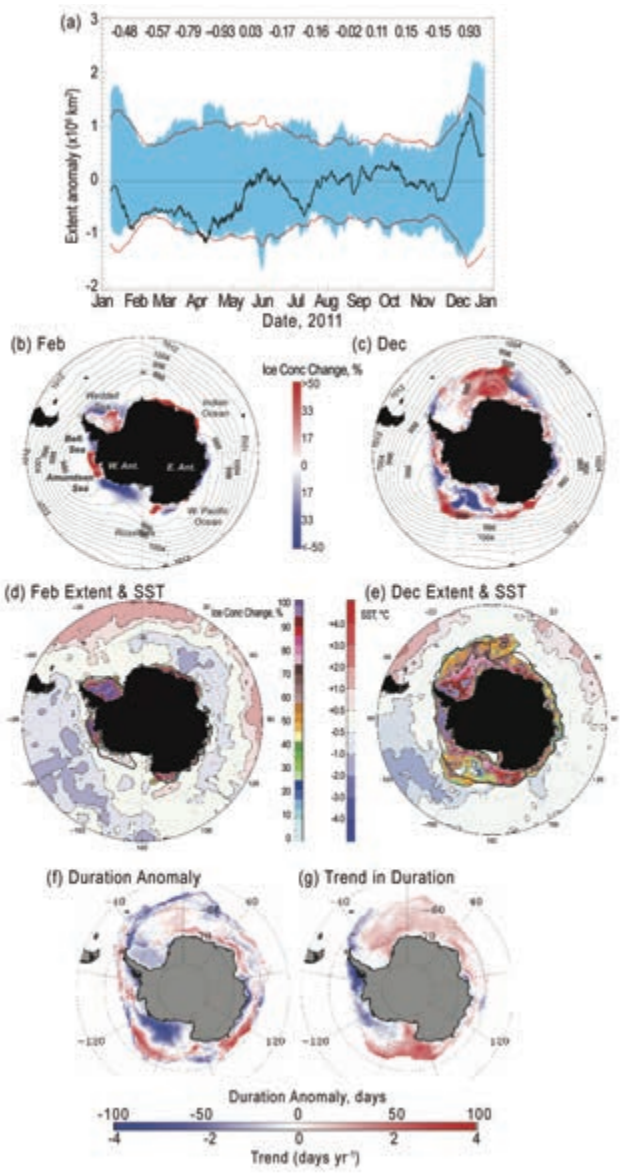

Fig. 6.8. (a) Plot of daily anomaly (black line) from the 1981–2010 climatology of daily Southern Hemisphere sea ice extent for 2011, based on satellite passive microwave ice concentration data from the GSFC Bootstrap Version 2 dataset (Comiso 1999). Blue banding represents the range of daily values for 1981–2010, while the red line represents ±2 standard deviations. Figures at the top are monthly mean extent anomalies ($\times 10^6$ km^2). (b) and (c) Sea ice concentration anomaly maps for February and December 2011 derived versus the monthly means for 1981–2010, with monthly mean contours of ACCESS MSLP. (Bell is Bellingshausen Sea.) (d) and (e) Maps of monthly mean sea ice concentration for February and December 2011, respectively, with mean ice edge/extent contours for 1981–2010 (black lines) and SST anomaly contours superimposed. The SST anomalies were calculated against the 1981–2010 mean and are based on data from the Optimal Interpolation SST version 2 dataset (Reynolds et al. 2002; Smith et al. 2008). (f) Sea ice duration anomaly for 2011/12, and (g) duration trend (see Stammerjohn et al. 2008). Both the climatology (for computing the anomaly) and trend are based on 1981/82 to 2010/11 data (Comiso 1999), while the 2011/12 duration-year data are from the NASA Team Near-Real-Time Sea Ice (NRTSI) dataset (Maslanik and Stroeve 1999).

the tropical Pacific. These conditions brought about earlier-than-normal sea ice retreat in the eastern Bellingshausen, western Weddell, and southern Ross Sea regions, contrasting with later-than-normal retreat in the outer eastern Ross Sea, Amundsen Sea, and Indian Ocean regions. For the most part, the sea ice advance anomaly pattern in 2011 mirrored the previous year's retreat pattern (in 2010/11) in that where the 2010/11 sea ice retreat was early, the 2011 sea ice advance was late (in the southern Bellingshausen Sea, western Weddell Sea, eastern Antarctica between ~80°E–120°E, and southern Ross Sea). Conversely, where the 2010/11 sea ice retreat was late, the advance was early (in the outer Amundsen Sea, outer Ross Sea, Indian Ocean between ~40°E–80°E, and the West Pacific sector between ~120°E and 160°E).

Of particular interest during April–May was a rapid change from a strongly negative to positive sea ice extent anomaly in the eastern Ross Sea sector. This was a result of a combination of high cyclonic activity, cold air advection, fresh water influx into the mixed layer (precipitation), and cool SSTs.

During the second phase, from mid-May to mid-November, the zonally-averaged extent largely fluctuated about the mean, with the exception of a dip towards two standard deviations below the long-term mean from mid-June to mid-July (Fig. 6.8a). The intervening wintertime dip occurred largely as a result of a southward incursion of the ice edge along a broad front from the tip of the Antarctic Peninsula eastwards across the Indian Ocean sector and in the western Ross Sea, coinciding with a band of anomalously warm SSTs in that region (not shown). This major incursion of the ice edge south of the long-term mean largely persisted through November, but was counterbalanced after mid-July by strong positive ice extent and concentration anomalies elsewhere (e.g., across the southwestern Pacific Ocean sector east of 120°E, the Ross Sea, and the northwestern Weddell and Bellingshausen Sea—the latter against the long-term negative trend; Comiso 2010; Stammerjohn et al. 2012). During this phase, the general atmospheric circulation reflected a weakening from near-neutral (mid-year) to moderately strong negative

SAM conditions (during austral spring; Fig. 6.2) and generally positive surface pressure anomalies at higher latitudes (Fig. 6.3e). As a consequence, the sea ice retreat anomaly pattern in 2011/12 was marked by late retreat across the Weddell, West Pacific, and outer Ross Sea regions, more or less opposite to that observed in the 2010/11 season.

The final phase, from mid-November onwards (Fig. 6.8a), entailed a rapid change to a strongly positive zonally-averaged ice extent anomaly and coincided with strong positive SAM/La Niña conditions with a classic ZW3 pattern in atmospheric pressure; low pressure centers in the eastern Weddell Sea, off East Antarctica at ~110°E, and in the Amundsen Sea (Figs. 6.2e; 6.8c). This resulted in the persistence of above-average ice extents and concentrations in the northeastern Weddell Sea, Ross Sea, and central West Pacific Ocean, plus near-average conditions elsewhere, with the exception of negative regional anomalies in the outer eastern Amundsen Sea, central Ross Sea, and northwestern Weddell Sea (Figs. 6.8c,e). The anomalously extensive sea ice in the Ross Sea also coincided with a region of cooler-than-average SSTs at this time (Fig. 6.8e). Overall Antarctic sea ice extent in December 2011 was the fifth highest since satellite records began in 1979.

The persistence of heavy pack and fast ice conditions along the Indian Ocean coastal sector during December continued to severely affect shipping operations and the resupply of Mawson Station (~62.9°E, 67.6°S). Conversely, in February, a strong storm in the McMurdo Sound area removed multiyear fast ice completely, during the early period of lower-than-normal sea ice extent in the southern Ross Sea. This resulted in damage to the ice pier at McMurdo Station, and probably contributed to the calving of two large icebergs from the McMurdo Ice Shelf at the southern end of the sound.

Given the midyear transition in the atmospheric circulation and sea ice anomaly patterns, the resulting sea ice season duration showed generally weak anomalies (Fig. 6.8f) overall (compared to 2010/11, for example). This was due to the fact that sea ice advance and retreat anomalies in most regions largely canceled each other out. In the western Weddell Sea, for example, the annual advance was late but the retreat was also late, so the ice season duration was near normal [relative to the long-term trends (Fig. 6.8g); see also Stammerjohn et al. 2012]. Greatest differences in 2011/12 compared to the long-term trends in annual sea ice season duration occur in the inner eastern Ross Sea (more strongly negative in 2011/12) and the relatively narrow zone in the Indian Ocean sector between ~110°E and 150°E (more strongly positive). The notable regional "hot-spot" of a long-term trend towards shortening of the sea ice season in the Amundsen-Bellingshausen Sea was less extensive in 2011/12 (Figs. 6.8f,g). Although ice extent and concentration anomalies were negative in this region in the first half of the year (in line with the long-term trend; Comiso 2010), the switch to positive anomalies for the remainder of the year created a near-zero duration anomaly for 2011/12.

g. *Ozone depletion*—P. A. Newman, E. R. Nash, C. S. Long, M. C. Pitts, B. Johnson, M.L. Santee, J. Burrows, and G. O. Braathen

The Antarctic ozone hole was moderately more severe in 2011 compared to the 1990–2011 period (average taken after the marked depletion in the 1980s). Figure 6.9 displays select October averages of total ozone derived from NASA instruments between 1970 and 2011. Prior to 1980 (top row), severe ozone depletion over Antarctica was not apparent. After 1990, nearly every year has seen a severe loss. As is clear from the bottom right panel (2011),

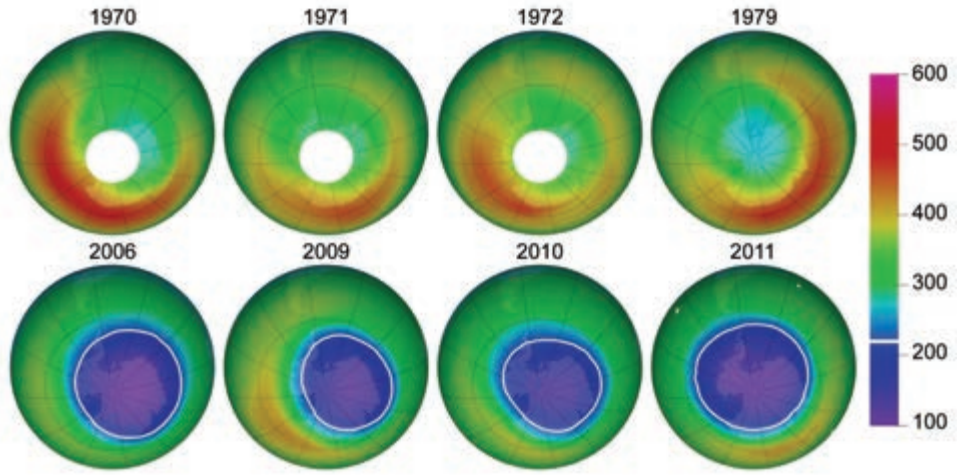

Fig. 6.9. October averages of total column ozone (Dobson Units, DU) derived from the Nimbus-4 BUV (1970–72), Nimbus-7 TOMS (1979), and OMI instruments (2006, 2009–11). The white line denotes the 220 DU (a nominal indicator of ozone depletion). Images courtesy of NASA (see http://ozonewatch.gsfc.nasa.gov).

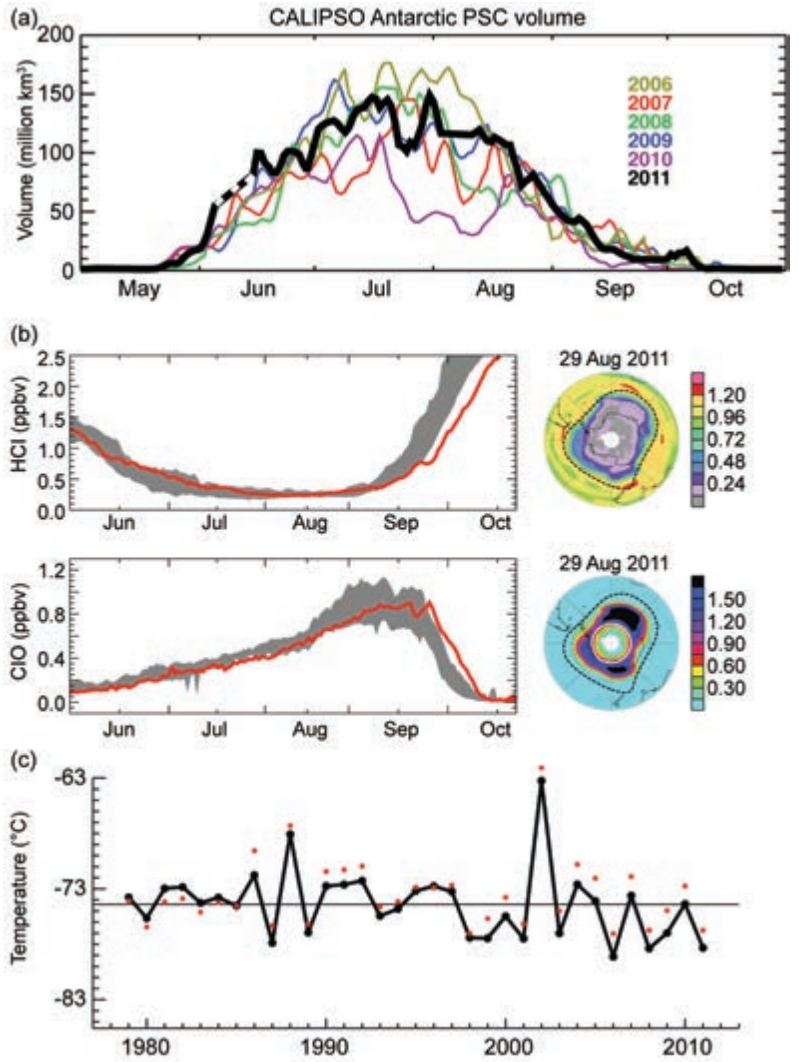

Fig. 6.10. (a) Daily time series of CALIPSO PSC volume for the Antarctic winter season (updated from Pitts et al. 2009). (b) HCl (top panel) and ClO (bottom panel) vortex-averaged time series on the 485K (~21 km, or 40 hPa) potential temperature surface from the Aura MLS in ppbv. The dashed black contour shown on the maps denotes the vortex edge. Gray shading on left denotes range of Aura MLS measurements during 2005–10, while red lines denote the 2011 values. The white circle on the ClO map shows the edge of polar night at local noon (updated from Manney et al. 2011). (c) September monthly mean temperature at 50 hPa, 60°S–90°S from MERRA data (black points and line) and NCEP/DOE data (red points). The MERRA data are biased 1°C colder than the NCEP/DOE data (Rienecker et al. 2011). In 2011, the average temperature was about 4°C below both the MERRA average and the NCEP/DOE average.

the Antarctic ozone loss in this past year was both deep and expansive.

The Antarctic ozone hole's area and depth are typically used as severity metrics. The area usually peaks in mid-September to early October. In 2011, the daily maximum area measured by the Ozone Monitoring Instrument (OMI) peaked at 26.0 million km^2 on 12 September. The time-averaged area (7 September to 13 October) was 24.7 million km^2. This made the 2011 ozone hole the seventh largest ozone hole over the 1990–2011 period (the 2006 ozone hole was the largest at 26.6 million km^2). The average depth of the 2011 ozone hole was 106 Dobson Units (DU)—averaged over the period of lowest ozone from 21 September to 16 October (the lowest OMI value was 95 DU on 8 October). The 2011 polar vortex was long lived, keeping the ozone hole near or above daily maximum values from mid-September through mid-November of previous years. Using a 15 September–30 November area average, 2011 was the second largest area in the 1990–2011 period (2006 was the largest for this period). Analyses from the SBUV and GOME-2 satellite instruments provide confirmation of these ozone hole estimates, albeit with slight differences due to instrument and retrieval differences.

Atmospheric profiles of ozone over Antarctica during early October 2011 show 100% depletion. Ozonesonde measurements on 9 October 2011 from South Pole show 98% ozone depletion in the 14 km – 21 km altitude range. Profile observations from satellites also reveal this severe ozone loss. Aura satellite observations from the Microwave Limb Sounder (MLS) instrument reveal that ozone decreased from above 3 ppmv to approximately 1 ppmv on the 485 K isentropic surface (about 40 hPa or 21 km) between 1 August and 1 October.

The ozone hole is caused by the conversion of chlorine molecules from nonreactive forms into ozone-destroying forms on the surfaces of particles in polar stratospheric clouds, or PSCs (i.e., $HC1+C1ONO_2 \xrightarrow{PSC} C1_2 + HNO_3$). The molecular chlorine photolyzes as the sun rises in spring, and this chlorine (combined with bromine) directly causes catalytic ozone loss. Figure 6.10a shows CALIPSO satellite observations of total PSC volume during the May–October period for six years. The May–October 2011 season showed the third largest average PSC volume (updated from Pitts et al. 2009).

The Aura MLS measures nonreactive HCl (Fig. 6.10b, top panels) and ozone-destroying ClO (Fig. 6.10b, bottom

panels). It is thus able to track the activation and deactivation of chlorine. The June–July HCl decreases as temperatures cool and PSCs form. As noted in the above equation, PSCs convert HCl and $ClONO_2$ into reactive chlorine (mainly ClO and Cl_2O_2). The resultant June–August ClO increase occurs because of this conversion. ClO peaks in September from the continued presence of PSCs and the rising sun over Antarctica. In late September, the complete destruction of ozone and evaporation of PSCs causes ClO (rapid decrease) to be converted back to HCl (rapid increase). As the right panels of Fig. 6.10b show, lower HCl and higher ClO than usual were found inside the 2011 Antarctic polar vortex. The high values of ClO and low values of HCl were unusually persistent in 2011 compared to MLS climatology. Time series of SCIAMACHY satellite observations of OClO and NO_2 show persistently high values of OClO and low NO_2 into October 2011, consistent with the higher MLS ClO. The higher ClO and OClO, combined with persistently low NO_2, enhanced conditions for ozone depletion in 2011, consistent with the relatively large extent of the Antarctic ozone hole during October. Ozone-depleting substances in the 2011 Antarctic ozone hole have only decreased by about 0.2 ppb from peak levels in the 2000–02 period of 4.0 ppb. This amounts to a 12% drop towards the 1980 level of 2.1 ppb.

Temperature variability of the Antarctic stratosphere modulates the year-to-year ozone hole severity. Below-average (above-average) Antarctic temperatures result in large and deep (small and shallow) ozone holes. Figure 6.10c shows Antarctic (60°S–90°S) September 50 hPa monthly mean temperatures. September 2011 was 4°C below average, and therefore consistent with higher levels of PSCs and greater chlorine activation (see also Fig. 6.2b).

The Antarctic stratosphere is warmed by the return of sunlight at the end of the polar winter and by large-scale weather systems (planetary-scale waves) that form in the troposphere and move upward into the stratosphere. The deposition of easterly momentum from these waves decelerates the polar night jet and causes a poleward and downward circulation. This downward circulation adiabatically warms the Antarctic lower stratosphere. During the 2011 Antarctic winter and spring, there were relatively weak wave events. This resulted in a colder-than-normal Antarctic vortex (as shown in Figs. 6.10c and 6.2b) and an unusually persistent Antarctic ozone hole. Low ozone values (< 220 DU) were observed until 21 December 2011.

Libraries: Please file with the *Bulletin of the American Meteorological Society*, Vol. 93, Issue 7